Journal of Materials Chemistry C

Single-component organic molecular ferroelectrics based on disk- or wheel-like rotation

Single-component organic molecular ferroelectrics

based on disk- or wheel-like rotation

Sachio Horiuchi[1], Reiji Kumai[2], and Shoji Ishibashi[3]

[1]Research Institute for Advanced Electronics and Photonics (RIAEP), National Institute of Advanced Industrial Science and Technology (AIST), AIST Tsukuba Central 5, 1-1-1 Higashi, Tsukuba, Ibaraki 305-8565, Japan

[2] Institute of Materials Structure Science, High Energy Accelerator Research Organization (KEK), Tsukuba 305-0801, Japan

[3]Research Center for Computational Design of Advanced Functional Materials (CD-FMat), National Institute of Advanced Industrial Science and Technology (AIST), AIST Tsukuba Central 2, Tsukuba 305-8568, Ibaraki, Japan

Abstract: Large polarizations and their reversible switching, which are indispensable for many functional ferroelectric applications, are achieved in new single-component organic molecular ferroelectrics with rotating strongly dipolar molecules or substituents. In a pre-screening process using a crystal structural database, both local-molecular and whole-crystal symmetries are inspected for the existence of pseudosymmetry required for rotational ferroelectricity, revealing several candidates: disk-type rotation in 1,2,3,4,5-pentamethyl-6-nitrobenzene (PMNB) molecules and wheel (or rotary knob)-type rotations of the substituents of 2-(methylsulfonyl)malonamide (MSMA), tris(4-acetylphenyl)amine (TAPA), and 4-methylsulfonyl-2-nitrotoluene (MSNT) crystals. The theoretically computed polarizations successfully reproduce experimental values, demonstrating that the rotational processes reverse most of the observed macroscopic polarizations. The theoretically large polarizations (7–8 $\mu C/cm^2$) being comparable to those of polymer ferroelectrics are attributed to the strongly electron-withdrawing nitro group in PMNB as well as the methylsulfonyl group of MSMA and MSNT being highly polarized in the radial direction.

1 Introduction

Ferroelectrics, which feature electrically switchable spontaneous polarizations, are the key functional materials for modern capacitors, memories, sensors, photonic devices, actuators, and energy harvesting devices, among others.[1–2] Their materials design must satisfy two structural

requirements. The first requirement is the existence of polarity; the crystal structure must be polar and should belong to one of ten polar point-group symmetries: 1 (C_1)*, 2 (C_2)*, m (C_{1h}), $mm2$ (C_{2v}), 4 (C_4)*, $4mm$ (C_{4v}), 3 (C_3)*, $3m$ (C_{3v}), 6 (C_6)*, or $6mm$ (C_{6v}), where an asterisk denotes a chiral point group.[1] Thus, all ferroelectrics exhibit piezoelectricity. The other requirement is the reversibility of polarity, which is enabled by the spatial degrees of freedom and makes the development of ferroelectric materials challenging. Whereas conventional chemical approaches to developing molecular-based ferroelectric materials[3-7] include the relative displacement of atoms/ions/molecules, reorientation of permanent dipoles, and proton transfer, some literatures report on intriguing examples of electronic ferroelectricity, where electron flow plays a dominant role in polarization.[8-10] Many of organic molecular solids and liquid crystals exhibit ferroelectricity because of the order–disorder-type reorientation of dipolar molecules or substituents, as exemplified by polyvinylidene fluoride and nylons. Very few of these materials had been reported to exhibit large spontaneous polarizations before polar globular rotators were incorporated into molecular or ionic crystals within the past decade.[11-16]

In general, effective methodologies of decoding material-specific information are required to accelerate the screening of target functional materials among numerous organic compounds. Ferroelectricity is a functionality that reveals a clear structure–property relationship. According to the aforementioned structural requirements, key information is the latent "pseudosymmetry", which can revive as the paraelectric structure.[17] The polarity of a polar crystal structure can be easily reversed when the crystal exhibits minimal deviation from centric symmetry. The structural information in the Cambridge Structure Database (CSD) has led to the discovery of several proton-transfer-type ferroelectrics.[18-20]

Here, we achieve high spontaneous polarizations that are switchable through rotations of disk- or wheel-shaped polar molecules/substituents. These discoveries are also based on structural assessments using the CSD. In our search for ferroelectric candidates, we began by screening for polar crystals in the CSD by narrowing the range of candidates to compounds with local pseudosymmetry based on the shape of a molecule or its substituents. Ferroelectric candidates are compounds in which this rotational disorder can revive the hidden symmetry of the whole crystal structure. The first target is an in-plane rotator, which enables disk rotation of whole polar molecules that exhibit a strong dipole moment. Some previous studies related to temperature-dependent permittivity detected antiferroelectric phase transitions, demonstrating the freezing of rotational motion in single- and binary-component antipolar molecular crystals of hexasubstituted benzene.[21-24] By contrast, in the present study, we extracted the structural information for a few polar crystals of disk-like hexasubstituted benzene molecules and found that one of them displayed ferroelectricity with high polarization. The second target is a wheel-type rotator. Recently, several ferroelectrics have been developed on the basis of a flip-flop motion of amide

groups, as exemplified by a series of columnar-type ferroelectric liquid crystals such as trialkylbenzene-1,3,5-tricarboxamide (BTA).[25-26] Its switching generally requires a very strong electric field to overcome the energic disadvantage stemming from the breaking of intermolecular NH···O hydrogen bonds. In the present study, we used a methylsulfonyl group as a strongly polarized rotator that does not form such intermolecular hydrogen bonds.

2 Experimental

2.1 Sample preparation

1,2,3,4,5-Pentamethyl-6-nitrobenzene (PMNB)[27] and tris(4-acetylphenyl)amine (TAPA)[28] were synthesized according to previously reported methods. 1-Methyl-4-methylsulfonyl-2-nitrobenzene (4-methylsulfonyl-2-nitrotoluene; MSNT) and 2-(methylsulfonyl)malonamide (MSMA) were purchased from Sigma-Aldrich and Organochem, respectively. Single crystals suitable for electric measurements were grown by recrystallization. Specifically, plate-like PMNB and TAPA were recrystallized by slow evaporation of 2-propanol and ethanol, respectively, elongated plates of MSMA crystals were recrystallized from methanol solution, and block-like MSNT crystals were recrystallized from ethanol solution. All these four compounds were stable against the air, moisture, and light.

2.2 Crystallographic studies

The X-ray diffraction studies have identified the single crystals of PMNB, TAPA, and MSNT as the reported polar crystal forms, respectively, and assigned the crystallographic axes for the electric measurements. Because only low-temperature (173 K) crystal-structure data are available for MSMA,[29] we determined its structure at room temperature for reference using a four-circle diffractometer (Rigaku AFC10) equipped with a hybrid pixel detector (PILATUS 200K) and a graphite-monochromated Mo Kα radiation source. The intensity data were analyzed using the CrystalStructure crystallographic software packages (Molecular Structure Corp. and Rigaku Corp.). The final refinements were carried out with anisotropic atomic displacement parameters for the nonhydrogen atoms and with a fixed C–H bond length of 0.95 Å for the hydrogen atoms.

2.3 Electric measurements

All of the electric measurements were conducted using single crystals with painted Ag paste as electrodes. The relative permittivity was measured using an LCR meter (Agilent, Precision E4980A). The electric polarization–electric field (P–E) hysteresis curves were recorded using the virtual ground method in conjunction with a ferroelectric evaluation system (Toyo Corp., FCE-1). The measurement system comprised a current/charge–voltage converter (Toyo Corp., model 6252), an arbitrary waveform generator (Biomation 2414B), an analogue-to-digital converter (WaveBook 516), and a voltage amplifier (NF Corp., HVA4321). All the crystals were immersed in silicone oil to avoid electric discharge. The longitudinal piezoelectric strain coefficient was

measured using a piezometer system (PM300, PiezoTest Ltd., UK) by the procedures described in our previous work.[30]

2.4 Theoretical evaluations

All of the calculations of electric polarizations were performed using the QMAS code[31] on the basis of the projector augmented-wave method [32] and using a plane-wave basis set. For the electronic exchange-correlation energy, the generalized gradient approximation of the Perdew–Burke–Ernzerhof form[33] was used. The hydrogen positions were computationally optimized because their accurate positions were not available from the results of X-ray diffraction measurements.

3 Results and Discussion

3.1 Structural assessment for disk-type ferroelectrics

In the present study, we selected hexasubstituted benzene molecules whose dipole moment can be enhanced by the asymmetric arrangement of strong electron-withdrawing and electron-donating groups. However, smooth molecular rotation of benzenes clearly requires approximate symmetry of sixfold rotation regarding the configuration of substituents. The structural prerequisite for ferroelectric molecular rotation is that the molecules not only have such the pseudo-rotational symmetry in shape individually but also occupy crystallographically pseudosymmetric sites. With these requirements in mind, we selected candidate molecules on the basis of the effective static shape of molecule drawn with van der Waals-type space-filling (i.e., Corey–Pauling–Koltun (CPK)) models.

As schematically illustrated in Supplementary Fig. S1(a), the axial symmetry has been examined by comparing the magnitude of projection (overhanging) along the radial direction of the rotator. For the tetragonal-shaped substituents –RXYZ or triangular-shaped –RXY, we define the distance Ω from the root carbon atom (C′) to the van der Waals surface of the terminal atom X as

$$\Omega = d(\text{C}'–\text{R}) − d(\text{R}–\text{X}) \cos \angle \text{C}'\text{RX} + r_v(\text{X}); \quad (1)$$

when X = CH_3,

$$\Omega = d(\text{C}'–\text{R}) − d(\text{R}–\text{C}) \cos \angle \text{C}'\text{RC} − d(\text{C}–\text{H}) \cos (\angle \text{RCH} − \angle \text{C}'\text{RC}) + r_v(\text{H}), \quad (2)$$

where d and r_v represent the bond lengths and the van der Waals radii taken from Bondi's compilation (1964),[34] respectively.

1,2,3,4,5-Pentamethyl-6-nitrobenzene (PMNB) is one of the polar disks assembled into the polar structure (Ref code PMNTBZ and PMNTBZ01).[35] Note that the NO_2 and CH_3 groups have Ω = 3.52 and 3.04 Å, respectively. This slight difference in Ω represents the nearly circular molecular shape, as evident from the space-filling drawing viewed normal to the plane (Fig. 1b). The crystal structure has the simplest unit cell comprising a single molecule ($Z = 1$) (Fig. 1c) and

4

belongs to the polar triclinic $P1$ (No. 1) space group. The flat disks are all located on the pseudo-inversion symmetry and are assembled into a thin sheet parallel to the crystallographic $(11\bar{1})$ plane. The uniform molecular arrangement is ideal for optimizing the spontaneous polarization, which can be reversed simply by the molecular disk rotation.

The CSD also includes an additional polar crystal of circular molecular disks; however, the electric properties of this material could not be examined. Pentachloroanisole crystallizes into a polar structure that belongs to the monoclinic $P2_1$ (No. 4) space group (Ref code FOYSAN). [36] The pseudosymmetry of centric space group $P2_1/n$ (No. 14) was detected as Alert level G in the validation of the CIF files using the *PLATON* program,[37] which is implemented as a part of the IUCr checkCIF facility. Unfortunately, the crystals were too fragile to be cut for the attachment of electrodes.

3.2 Structural assessment of wheel-type ferroelectrics

The second approach is to use axially asymmetric substituents as a wheel or a rotary knob. A large dipole moment can be induced by introducing electron-donating atom/group X and electron-withdrawing atom/group Y into tetragonal-shaped substituents –RXYZ or triangular-shaped substituents –RXY. The magnitude of projection (overhanging) along the radial direction of the rotator can be similarly argued as illustrated in Fig. S1(b). Here we define the radial distance Ω' from the rotation axis (including the C′–R bond) to the van der Waals surface of the terminal atom X as

$$\Omega' = d(\text{R–X}) \sin \angle\text{C′RX} + r_v(\text{X}); \quad (3)$$

when $X = CH_3$,

$$\Omega' = d(\text{R–C}) \sin \angle\text{C′RC} - d(\text{C–H}) \sin (\angle\text{RCH} + \angle\text{C′RC}) + r_v(\text{H}). \quad (4)$$

Here, we use two kinds of substituents and their axial rotation can flip the molecular dipoles. The methylsulfonyl –S(=O)$_2$CH$_3$ group has a dipole moment whose rotatable-direction component is parallel to the perpendicular bisector of the base of the isosceles triangle O_2C. The difference in Ω' between the oxygen and methyl components of a methylsulfonyl group (2.88 vs. 3.44 Å) is small, causing the pseudo-threefold rotation symmetry. A search for polar single-component molecular crystals with a methylsulfonyl group revealed crystalline 2-(methylsulfonyl)malonamide (MSMA)[29] as a ferroelectric candidate. The molecule has two amide groups and one methylsulfonyl group (Fig. 2a,b). The malonamide backbones drawn in blue and purple in the figure construct the rigid hydrogen-bonded network, whose cavity accommodates the methylsulfonyl group drawn in yellow and red (Fig. 2c). The crystal structure belongs to the orthorhombic space group $Pna2_1$ (No. 33). The malonamide backbones with pseudomirror symmetry (Fig. 2b) adopt the approximate local symmetry of space group $Pnam$ (No. 62). The corresponding pseudosymmetry was detected as Alert level G in the validation of the CIF files using the *PLATON* program. The spontaneous polarization being uniaxial and parallel to the *c*-

direction is a result of the asymmetric orientation of the dipolar methylsulfonyl groups, whose reorientation or rotation is thus expected to reverse the polarization.

A similar molecular dynamical approach is to exploit the acetyl group as a rotary knob. According to eqs. (3) and (4), the pseudo-twofold rotational symmetry of acetyl group appears as the small difference in Ω' between its oxygen and methyl moieties (2.63 vs. 3.21 Å), which is as small as the difference in Ω' between the oxygen and methyl moieties of the methylsulfonyl group. The TAPA molecules accommodate three acetyl groups, which are all bound to the terminals of the triphenylamine backbone, as highlighted by yellow and red in Fig. 3. The crystal structure (CSD RefCode: IDOKUI)[38] belongs to the orthorhombic space group $Pna2_1$ (No. 33) and exhibits a pseudo-twofold rotation axis, which is parallel to the b-axis and penetrates the triphenylamine core (Fig. 3c). Therefore, the triphenylene backbones exhibit the approximate symmetry of space group $Pnab$ (No. 60). The orientation of all the acetyl groups locally breaks this pseudosymmetry, and the total sum of the acetyl groups' dipoles is parallel to the c-direction. Therefore, polarization reversal requires revolving these flat rotary knobs.

The same argument is applicable to the fourth candidate, MSNT. The crystal structure of MSNT (CSD RefCode: MIGSUR) [39] belongs to the orthorhombic space group $Pca2_1$ (No. 29) having uniaxial polarity parallel to the c-direction (Fig. 4). The pseudocentric structure with space group $Pcam$ (No. 57) is constructed by the toluene unit, which occupies the pseudo-mirror symmetry parallel to the (001) plane. However, the orientations of the nitro and methylsulfonyl groups result in deviation from this mirror symmetry. Therefore, the crystal structure can be reversed by revolving both the nitro and methylsulfonyl groups as a thin rotary knob and a wheel, respectively. Note that only the methylsulfonyl group can contribute to the spontaneous polarization because the dipole moment of the axially symmetric nitro group has no radial direction component.

3.3 New ferroelectrics and their electric and thermal properties

The field-induced rotations of the molecules or the substituents expected in the previously discussed ferroelectric candidates have been confirmed by P–E hysteresis measurements at room or higher temperatures. The P–E curve of the PMNB crystal at room temperature exhibits a parallelogram shape (Fig. 5a) characteristic of ferroelectric behavior. It shows a large remanent polarization P_r of ~6 μC/cm^2 and a very high coercive field E_c of ~100 kV/cm at a frequency of 1 Hz when in an $E\|c^*$ configuration. This hysteresis loop collapses with increasing frequency because of an increase of the coercive field, which corresponds to the peak field of the corresponding current density (J)–E curves. The room-temperature ferroelectricity has been justified by the double-wave method, which can effectively eliminate the non-ferroelectric hysteresis components (see Fig. S2a-d). The switching rate is found to be thermally accelerated

as shown by the hysteresis at higher frequencies (10-30 Hz) at the higher temperature (see the data at T = 331 K in Fig. S2e).

The P–E hysteresis loops and the corresponding peak in the J–E curves of MSMA crystals at room temperature also indicate ferroelectricity (Fig. 5b). Because of the crystal habit, the direction of the applied electric field E is normal to the (011) plane and then inclined by 58.4° from the c-axis parallel to the polarization. Given this field configuration, a total polarization as large as 7.3 $\mu C/cm^2$ is deduced from the observed remanent polarization of 3.8 $\mu C/cm^2$. The observed high coercive field E_c of approximately 100–160 kV/cm at a frequency of 3–30 Hz is much smaller than those of hydrogen-bonded liquid-crystalline BTA (250–400 kV/cm). Both PMNB and MSMA crystals exhibit a nearly temperature-independent relative permittivity at temperatures near room temperature, indicating the absence of a Curie temperature (Fig. S3). Note that the phase transition was detected for PMNB via differential scanning calorimetry (DSC) measurements (Fig. S4) at temperatures greater than the measurement temperature range of permittivity, where the samples start to sublime. The DSC thermograms of PMNB show a pair of exothermal and endothermal peaks, which are attributed to the reversible phase transition at 403 K, representing likely the Curie temperature. The transition enthalpies ΔH (shown in the figure) on heating and cooling correspond to the transition entropies $\Delta S = \Delta H/T$ of 11.6 and 9.96 J/K mol, respectively. Such the large entropy changes can be explained by $\Delta S = R \ln g$ for the orientational order-disorder mechanism having possible g configurations in the disordered phase, where R is the gas constant (8.31 J/K mol). Therefore, the high-temperature phase of PMNB is expected to be a plastic crystal having g close to 4 ($R \ln 4$ = 11.5 J/K mol). In the thermograms of the MSMA, no phase transition is observed at temperatures as high as the melting point (495 K).

P–E hysteresis measurements were conducted at high temperatures for the TAPA and MSNT crystals, whose room-temperature measurements did not show hysteresis loops. The results for the TAPA crystal at T = 403 K reveal a hysteresis loop characteristic of a ferroelectric and an E_c of approximately 60–70 kV/cm at a frequency of 10–20 Hz (Fig. 6a). The direction of the applied electric field E is normal to the (011) plane. As shown in Fig. 6b and 6c, the coercive field E_c defined at the peak of the J–E curve decreases with increasing temperature until the peak suddenly disappears at 408 K. Such the linear temperature dependence of E_c is a typical characteristic of a ferroelectric-to-paraelectric transition.[40] As expected, the DSC measurements reveal corresponding exothermal and endothermal peaks at T = 402 K and 408 K (Fig. S4). The observed large entropy change $\Delta S = \Delta H/T$ of 8.52 and 10.1 J/K mol on heating and cooling, respectively, can be related to the order-disorder mechanism with g = 2.8 and 3.4. All of the P–E curves show longitudinal warp; consequently, the P_r value obtained from the upper P–E loops (top panel of Fig. 6a), 2–3 $\mu C/cm^2$, is overestimated. This overestimation is attributed to the undesirable contribution of the dc (leakage) current $J_{dc}(E)$, as evident from the J–E curve (upper curves in

bottom panel). The slope of the inclined J–E curve corresponds to the conductivity. The genuine ferroelectric polarizations should be extracted by subtracting the $J_{dc}(E)$ from the J–E curve. Here, $J_{dc}(E)$ was assumed to include a nonlinear term as $J_{dc}(E) \propto (E + \alpha E^3)$, which was fitted to the J–E curve at the backward-voltage-sweeping stage. The P–E and J–E curves in bottom of each panel of Fig. 6a represent the corrected data. The parallelogram-shaped P–E loops yielded a moderate magnitude of the P_r (1.3 μC/cm^2), which corresponds to a total polarization of 1.6 μC/cm^2 along the c-direction. The direct piezoelectric effect with longitudinal coefficient d = -3.6 pC/N has been also observed on the electrically poled TAPA crystal by applying stress normal to (011) plane.

The J–E curves of MSNT (Fig. 7a) show a similar temperature dependence as those of TAPA. This finding suggests ferroelectric behavior at temperatures immediately below the melting point (T = 392 K), which was identified by the DSC measurement results (Fig. S4). The data also show a substantial contribution of the dc current density $J_{dc}(E)$. From the T = 388 K data, we extracted the intrinsic ferroelectric polarization by subtracting the $J_{dc}(E)$ from the J–E curve. The parallelogram-shaped P–E hysteresis loop typical of a ferroelectric is accompanied by approximate spontaneous polarization of 9.5 ± 1.5 μC/cm^2 given the ambiguity of the fitting (Fig. 7b).

3.4 Theoretical evaluation of polarizations

To verify the aforementioned mechanisms of the polarization reversal, we simulated the spontaneous polarizations using density functional theory calculations in combination with the modern (Berry phase) theory of polarization.[41,42] The experimentally measured values correspond to polarization changes ΔP during the structural change from the initial (reference) to the final (target) state. The spontaneous polarization in displacive- or proton-transfer-type ferroelectrics is conventionally obtained by simulating the polarization change $\Delta P(\lambda)$ as a function of the degree of polar distortion λ from the (real or hypothetical) paraelectric reference structure with $\lambda = 0$ and $P = 0$.[19,43] Hypothetical structures for intermediate λ values that ensure smooth variations of P were obtained by linear interpolation of the two structures at $\lambda = 0$ and 1. By contrast, for the rotational-type ferroelectrics investigated in the present work, the corresponding $\lambda = 0$ reference structure is unavailable because an ill-defined structure is formed by averaging the atomic coordinates between the ferroelectric ($\lambda = 1$) and its symmetry-inverted structures ($\lambda = -1$). Even if the $\lambda = 0$ structure data were available, the linear interpolation approach is not adequate to deduce intermediate λ structures for rotational-type ferroelectrics.

We evaluated the theoretical polarizations by calculating the polarization changes as a function of the axial rotation without passing the centrosymmetric $P = 0$ state. The left part of Figure 8a shows a plot of the polarization of PMNB as a function of the disk rotation angle θ, where $\theta = 0°$ corresponds to the $\lambda = 1$ structure. Its inversion structure is the $\lambda = -1$ structure,

which can be smoothly connected to the structure rotated by $\theta = 180°$ (Fig. 8a, right). The origin of polarization is set such that $\boldsymbol{P}(\lambda = -1) = -\boldsymbol{P}(\lambda = 1)$. The total polarization $|\boldsymbol{P}|$ is 7.8 $\mu C/cm^2$ (~5.9 D), and the c^*-direction component of 7.6 $\mu C/cm^2$ at $\lambda = 1$ ($\theta = 0°$) and -1 can well explain the remanent polarization P_r of ~6 $\mu C/cm^2$ measured for the $\boldsymbol{E}\|c^*$ configuration.

Regarding the wheel (or rotary knob)-type substituents, the structural changes during the ferroelectric switching are divided into two processes for convenience: (1) the axial rotation of substituents and (2) additional minor rearrangement, including rearrangement of the host framework. Figure 8b depicts the c-direction component of polarization in the MSMA crystal. The methylsulfonyl group is tilted from pseudo-mirror symmetry by $\Delta\Phi = 51.9°$ at $T = 296$ K. The polarization change ΔP is first calculated as a function of the rotation angle φ of the methylsulfonyl group from $\varphi = 0°$ to $105°$ (~$2\Delta\Phi$) (left panel), and then linear extrapolation is used to describe the additional adjustment to the mirrored (target) structure. The origin of the polarization is the same as previously described. The calculated polarization P^{cal} is very large (8.1 $\mu C/cm^2$) and corresponds to an effective moment of 4.5 D. The plot indicates that the P^{cal} arises mostly from rotation of the methylsulfonyl group. The experimentally derived total polarization $|\boldsymbol{P}| = 7.3$ $\mu C/cm^2$ coincides with the P^{cal} within ~10% error. Note that the larger P^{cal} (8.7 $\mu C/cm^2$) was obtained for the low-temperature structure (173 K, RefCode MAJNES),[29] which exhibits greater deviation ($\Delta\Phi = 56°$) from the mirror symmetry.

Similar procedures were applied to simulate the polarizations in TAPA and MSNT crystals. The major contribution to the spontaneous polarization of 2.5 $\mu C/cm^2$ is caused by the $180°$ rotation of three acetyl groups of TAPA (Fig. 8c). This value is comparable to the experimentally derived value of 1.6 $\mu C/cm^2$. The calculated polarization of 7.0 $\mu C/cm^2$ in MSNT is obtained by $180°$ rotation of the methylsulfonyl and methyl groups and $90°$ rotation of the nitro group (Fig. 8d); this value is also similar to the aforementioned experimental estimate.

4 Conclusion

A structural assessment inspecting for the pseudosymmetries revealed ferroelectric candidates among compounds in the CSD and led us to a new avenue for developing organic ferroelectrics based on in-plane molecular rotators and substituent wheels (or rotary knobs). The theoretical simulation of polarizations successfully reproduced the experimental values, demonstrating that the rotational processes reverse a large portion of the observed macroscopic polarizations. Large theoretical polarizations (7–8 $\mu C/cm^2$) comparable to those of polymer ferroelectrics were obtained because the strongly electron-withdrawing nitro group in PMNB as well as the methylsulfonyl group of MSMA and MSNT is highly polarized in the radial direction. The ferroelectric phases are stable over a wide temperature range: the upper temperature limits correspond to the orientational order-disorder phase transitions at ~400 K for PMNB and TAPA

and to the melting point of MSMA (495 K) and MSNT (392 K). Whereas the phase transition mechanism of the former two compounds justifies the molecular rotational mechanism of ferroelectricity, thermal behaviors of the latter two compounds mean that the Curie temperature is not always appropriate for screening ferroelectricity. On the other hand, coexistence of local pseudo-*n*-fold rotational symmetry of the rotators and the whole-crystal pseudosymmetry can be the promising signs leading to hitherto hidden ferroelectric candidates. Indeed, the pseudo-*n*-fold rotational symmetry of the each molecular or substituent's shape appears as the small difference (0.48-0.58 Å) in the parameter Ω or Ω' which is defined as the magnitude of projection along the radial direction of the rotator. We believe that such decoding of material-specific information in conjunction with theoretical computing offers rich opportunities for discovering advanced ferroelectric materials.

Conflicts of interest

There are no conflicts of interest to declare.

† Electronic Supplementary Information (ESI) available: Additional structural information, CIF file, and additional data of dielectric and thermal properties. CCDC-2093843. For ESI and crystallographic data in CIF see DOI: 10.1039/x0xx00000x

References

1) M. E. Lines and A. M. Glass, *Principles and Applications of Ferroelectrics and Related Materials*, Oxford University Press, New York, 1977.

2) K. Uchino, *Ferroelectric Devices*, Marcel Dekker, New York, 2000.

3) S. Horiuchi and Y. Tokura, *Nat. Mater.*, 2008, **7**, 357–366.

4) T. Hang, W. Zhang, H.-Y. Ye and R. G. Xiong, *Chem. Soc. Rev.*, 2011, **40**, 3577–3598.

5) A. S. Tayi, A. Kaeser, M. Matsumoto, T. Aida and S. I. Stupp, *Nat. Chem.*, 2015, **7**, 281–294.

6) S. Horiuchi and S. Ishibashi, *J. Phys. Soc. Jpn.*, 2020, **89**, 051009.

7) H. L. B. Boström and A. L. Goodwin, *Acc. Chem. Res.*, 2021, **54**, 1288–1297.

8) S. Ishibashi and K. Terakura, *J. Phys. Soc. Jpn.*, 2014, **83**, 073702.

9) K. Terakura and S. Ishibashi, *Phys. Rev. B*, 2015, **91**, 195120.

10) S. Kuniki, S. Ohmura and A. Takahashi, *Phys. Rev. B*, 2018, **98**, 165149.

11) J. Harada, T. Shimojo, H. Oyamaguchi, H. Hasegawa, Y. Takahashi, K. Satomi, Y. Suzuki, J. Kawamata and T. Inabe, *Nat. Chem.*, 2016, **8**, 946–952.

12) H. Y. Ye, Y. Y. Tang, P. F. Li, W. Q. Liao, J. X. Gao, X. N. Hua, H. Cai, P. P. Shi, Y. M. You and R. G. Xiong, *Science*, 2018, **361**, 151–155.

13) J. Harada, Y. Kawamura, Y. Takahashi, Y. Uemura, T. Hasegawa, H. Taniguchi and K. Maruyama, *J. Am. Chem. Soc.* 2019, **141**, 9349–9357.

14) H. Morita, R. Tsunashima, S. Nishihara, K. Inoue, Y. Omura, Y. Suzuki, J. Kawamata, N. Hoshino and T. Akutagawa, *Angew. Chem. Int. Ed.*, 2019, **58**, 9184–9187.

15) P. -F. Li, W.-Q. Liao, Y.-Y. Tang, W. Qiao, D. Zhao, Y. Ai. Y.-F. Yao and R.-G. Xiong, *Proc. Natl. Acad. Sci. U. S. A.*, 2019, **116**, 5878–5885.

16) Y. Ai, Y. -L. Zeng, W. -H. He, X. -Q. Huang, Y. -Y. Tang, *J. Am. Chem. Soc.*, 2020, **142**, 13989–13995.

17) S. C. Abrahams, *Ferroelectrics*, 2011, **104**, 37–51.

18) S. Horiuchi, R. Kumai and Y. Tokura, *Adv. Mater.*, 2011, **23**, 2098–2103.

19) S. Horiuchi, K. Kobayashi, R. Kumai and S. Ishibashi, *Nat. Commun.*, 2017, **8**, 14426.

20) S. Horiuchi, F. Kagawa, K. Hatahara, K. Kobayashi, R. Kumai, Y. Murakami and Y. Tokura, *Nat. Commun.*, 2012, **3**, 1308.

21) Y. Balcou and J. Meinnel, *J. Chim. Phys. Phys.-Chim. Biol.*, 1966, **63**, 114–120.

22) J. Harada, M. Ohtani, Y. Takahashi and T. Inabe, *J. Am. Chem. Soc.*, 2016, **137**, 4477–4486.

23) J. Ichikawa, N. Hoshino, T. Takeda and T. Akutagawa, *J. Am. Chem. Soc.*, 2015, **137**, 13155–13160.

24) J. Harada, N. Yoneyama, S. Sato, Y. Takahashi and T. Inabe, *Cryst. Growth Des.*, 2019, **19**, 291–299.

25) C. F. C. Fitié, W. S. C Roelofs, M. Kemerink and R. P. Sijbesma, *J. Am. Chem. Soc.*, **132**, 2010, 6892–6893.

26) I. Urbanaviciute, X. Meng, T. D. Cornelissen, A. V. Gorbunov, S. Bhattacharjee, R. P. Sijbesma and M. Kemerink, *Adv. Electron. Mater.*, 2017, **3**, 1600530.

27) G. A. Olah, A. P. Fung, S. C. Narang and J. A. Olah, *J. Org. Chem.*, 1981, **46**, 3533–3537.

28) J. Wang, C. He, P. Wu, J. Wang and C. Duan, *J. Am. Chem. Soc.*, 2011, **133**, 12402–12405.

29) A. Basheer, M. Mishima and Z. Rappoport, *J. Phys. Org. Chem.*, 2010, **23**, 255–265.

30) S. Horiuchi, J. Tsutsumi, K. Kobayashi, R. Kumai, S. Ishibashi, *J. Mater. Chem. C*, 2018, **6**, 4714-4719

31) S. Ishibashi, T. Tamura, S. Tanaka, M. Kohyama and K. Terakura, *Phys. Rev. B*, 2007, **76**, 153310.

32) P. E. Blöchl, *Phys. Rev. B*, 1994, **50**, 17953–17979.

33) J. P. Perdew, K. Burke and M. Ernzerhof, *Phys. Rev. Lett.*, 1996, **77**, 3865–3868.

34) A. Bondi, *J. Phys. Chem.*, 1964, **68**, 441–451.

35) Y. V. Gatilov, N. G. Bokii and Y. T. Struchkov, *J. Struct. Chem.*, 1975, **16**, 654–656.

36) K. Rissanen, J. Valkonen and J. Knuutinen, *Acta Crystallogr., Sect. C: Cryst. Struct. Commun.*, 1987, **43**, 1966–1968.

37) A. L. Spek, *J. Appl. Cryst.*, 2003, **36**, 7–13.

38) C. M. Cui, H. P. Zhou, C. H. Zhu and J. Y. Wu, *Acta Crystallogr., Sect. E: Crystallogr. Commun.*, 2006, **62**, o1762–o1763.

39) Q-A. Wu, W.-M. Fang, D.-W. Luo and Z.-Y. Xu, *Acta Crystallogr., Sect. E: Struct. Rep. Online*, 2007, **63**, o3320–o3320.

40) L. Jin, F. Li, and S. Zhang, *J. Am. Ceram. Soc.* **2014**, 97, 1-27.

41) R. Resta, *Rev. Mod. Phys.*, 1994, **66**, 899–915.

42) R. D. King-Smith and D. Vanderbilt, *Phys. Rev. B*, **1993**, 47, 1651–1654.

43) S. Ishibashi and K. Terakura, *Phys. B (Amsterdam, Neth.)*, 2010, **405**, S338–S340.
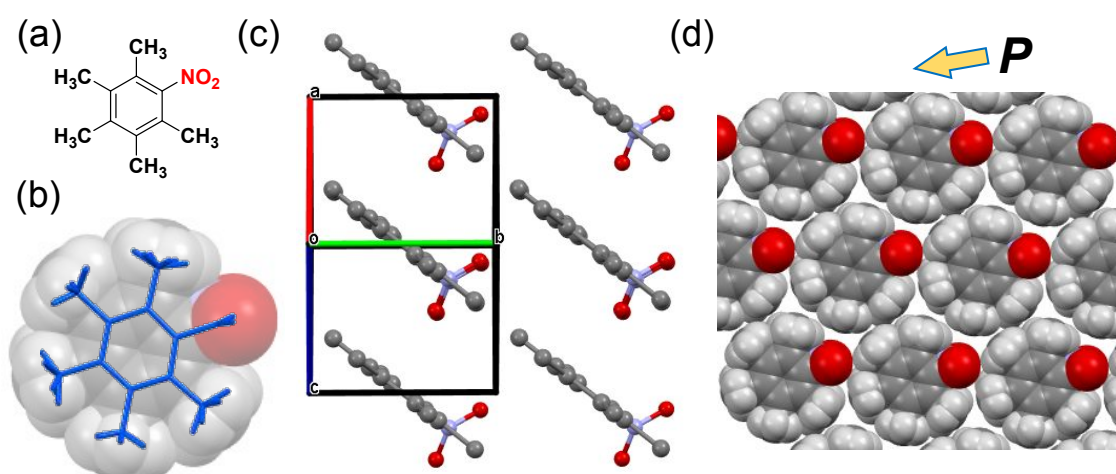
Figure 1   1,2,3,4,5-Pentamethyl-6-nitrobenzene (PMNB): (a) chemical structure; (b) molecular structures displayed as superimposed space-filling and stick models; (c) crystal structures viewed along the [101] direction; and (d) the space-filling model of a molecular sheet viewed along the [11$\bar{1}$] direction. The atomic coordinates are from the CSD Ref. Code PMNTBZ01.
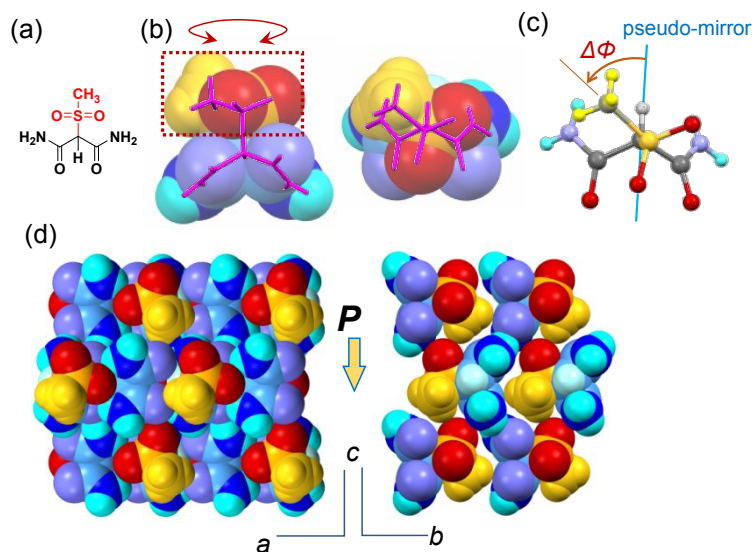
Figure 2 2-(Methylsulfonyl)malonamide (MSMA): (a) chemical structure; (b) molecular structures displayed as superimposed space-filling and stick models; and (c) crystal structures viewed along the *b*- (left panel) and *a*-directions (right panel). Methylsulfonyl groups are highlighted by yellow and red spheres.
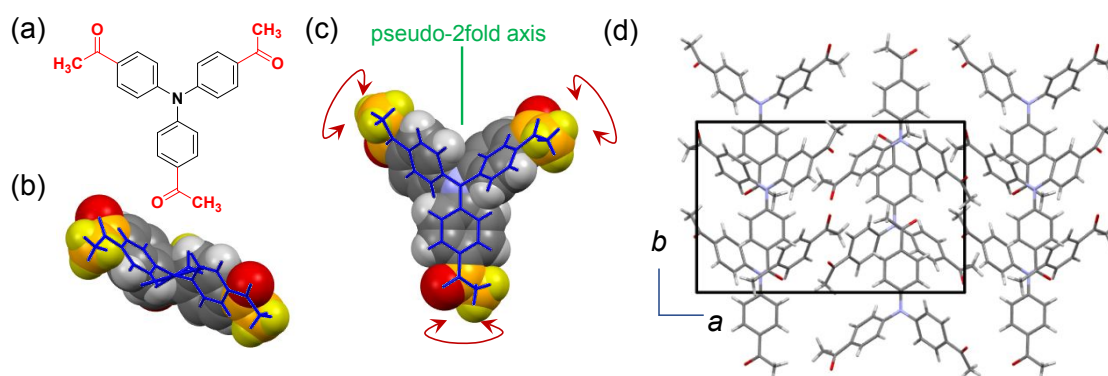
Figure 3 Tris(4-acetylphenyl)amine (TAPA): (a) chemical structure; (b,c) molecular structures displayed as superimposed space-filling and stick models viewed (b) parallel and (c) normal to the pseudo-twofold axis; and (d) crystal structures viewed along the *c*-direction. Acetyl groups are highlighted by yellow and red spheres. The atomic coordinates are from the CSD Ref. Code IDOKUI.
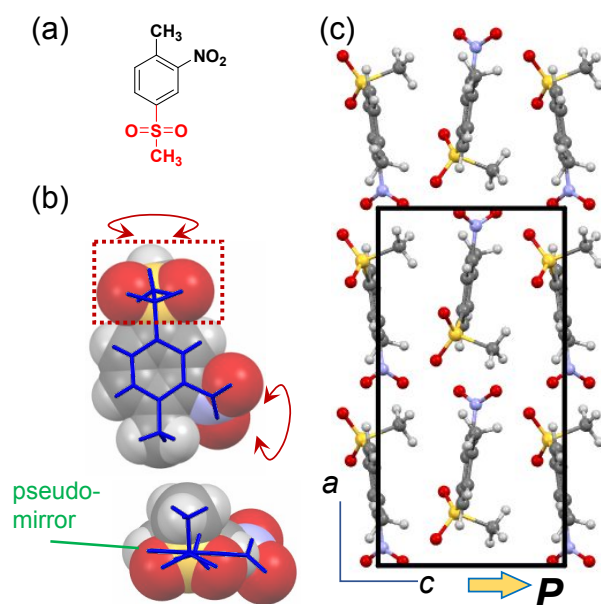
Figure 4   4-Methylsulfonyl-2-nitrotoluene (MSNT): (a) chemical structure; (b) molecular structures displayed as superimposed space-filling and stick models; and (c) crystal structures viewed along the *b*-direction. Sulfonyl groups are highlighted by yellow and red spheres. The atomic coordinates are from the CSD Ref. Code MIGSUR.
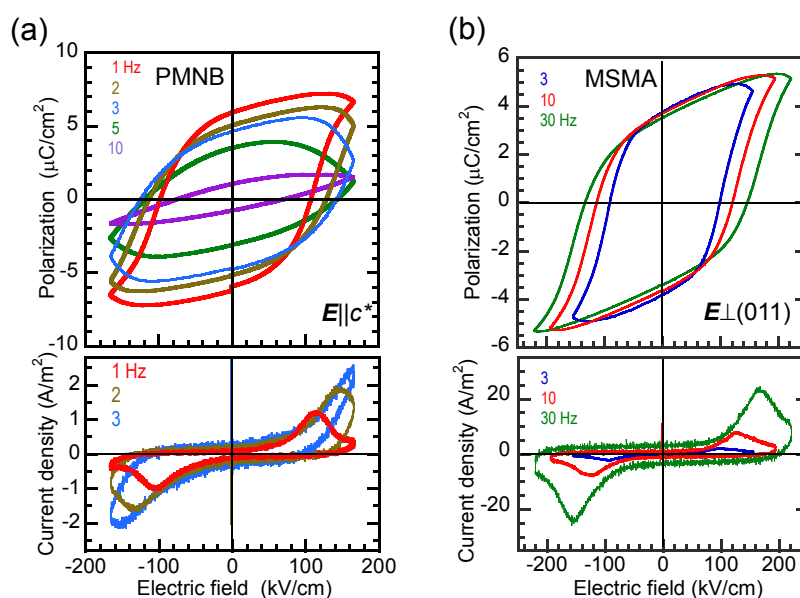
Figure 5   Room-temperature ferroelectricity: (top) *P–E* hysteresis loops and (bottom) the corresponding *J–E* curves measured with *E* of various frequencies applied (a) along the *c**-direction of a PMNB single crystal and (b) normal to the (011) surface of an MSMA crystal.
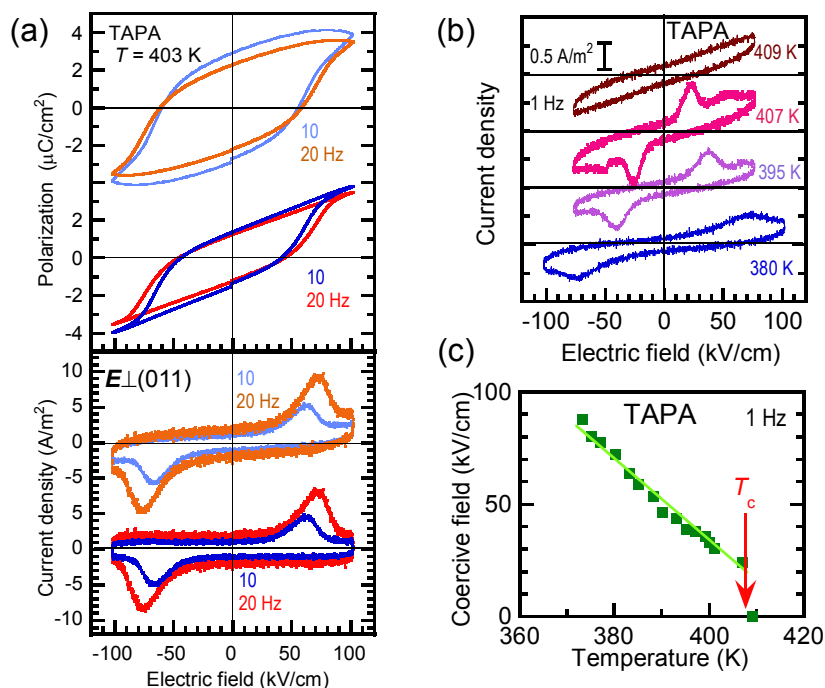
Figure 6   High-temperature ferroelectricity of TAPA: (a) *P–E* hysteresis loop (top panel) and the corresponding *J–E* curve (bottom panel) measured with *E* applied normal to the (011) surface at *T* = 403 K. In each panel, the upper and lower curves represent raw and corrected data, respectively. (b) The thermal evolution of the *J–E* curves and (c) the temperature dependence of the coercive field defined at the peak of the *J–E* curves.
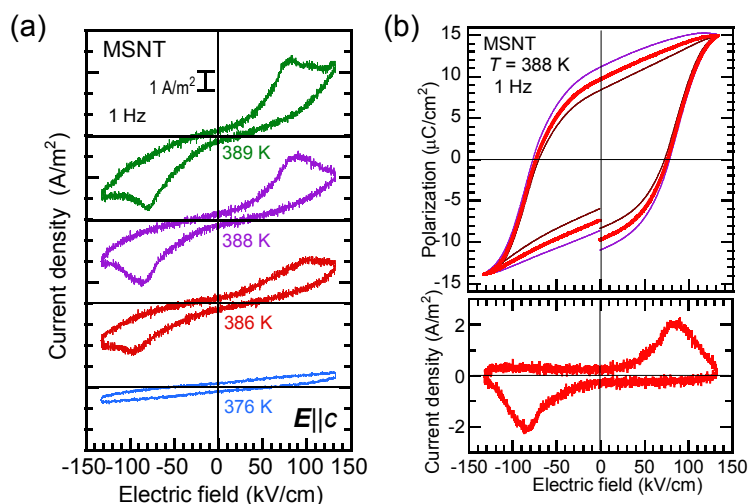
Figure 7   High-temperature ferroelectricity of MSNT: (a) *J–E* curves with *E* applied along the *c*-direction at temperatures immediately below the melting point; (b) the corrected *P–E* hysteresis curves (top panel) and *J–E* curves (bottom panel) at *T* = 388 K and 1 Hz.
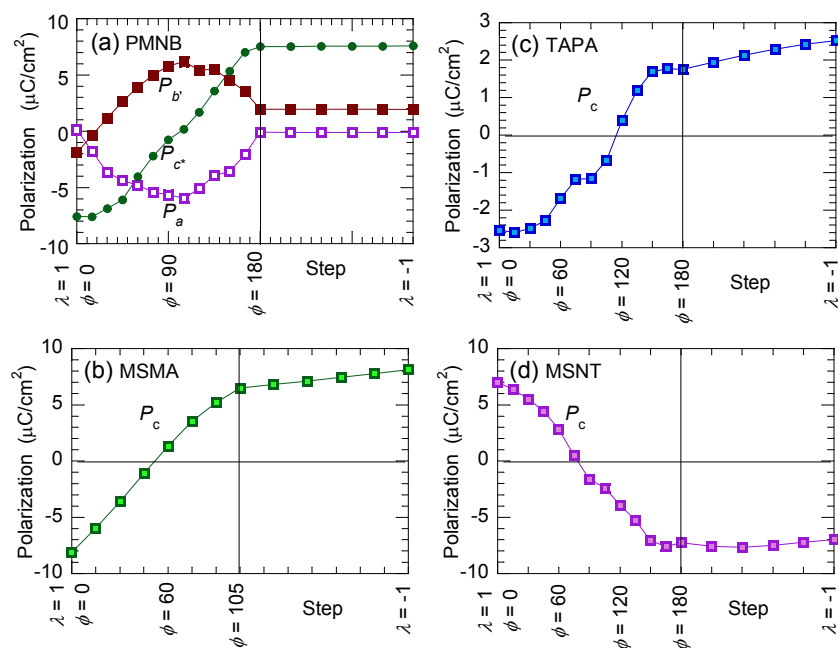
Figure 8 Variation of the theoretical polarizations as a function of structural changes from the fully polarized (ferroelectric, degree of distortion $\lambda = 1$) to its reversed configuration ($\lambda = -1$). (a) Total polarization and its direction components of PMNB as a function of disk rotation angle θ. (b–d) Total polarization parallel to the c-direction of (b) MSMA, (c) TAPA, and (d) MSNT. Each left part represents the rotation process of polar substituents from the $\lambda = 1$ structure, whereas each right part corresponds to the additional adjustment process to the symmetry-inverted $\lambda = -1$ structure.